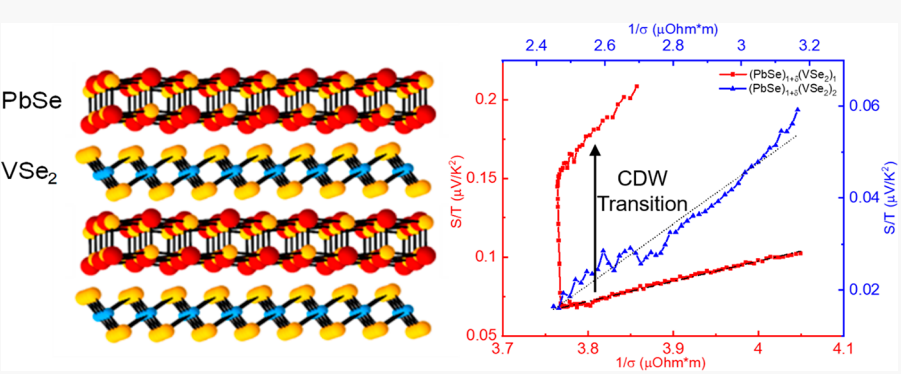


pubs.acs.org/NanoLett Letter

Enhanced Low-Temperature Thermoelectric Performance in $(PbSe)_{1+\delta}(VSe_2)_1$ Heterostructures due to Highly Correlated Electrons in Charge Density Waves

Yu Wang, Danielle M. Hamann, Dmitri Leo M. Cordova, Jihan Chen, Bo Wang, Lang Shen, Zhi Cai, Haotian Shi, Evguenia Karapetrova, Indu Aravind, Li Shi, David C. Johnson, and Stephen B. Cronin*





ABSTRACT: We explore the effect of charge density wave (CDW) on the in-plane thermoelectric transport properties of $(PbSe)_{1+\delta}(VSe_2)_1$ and $(PbSe)_{1+\delta}(VSe_2)_2$ heterostructures. In $(PbSe)_{1+\delta}(VSe_2)_1$ we observe an abrupt 86% increase in the Seebeck coefficient, 245% increase in the power factor, and a slight decrease in resistivity over the CDW transition. This behavior is not observed in $(PbSe)_{1+\delta}(VSe_2)_2$ and is rather unusual compared to the general trend observed in other materials. The abrupt transition causes a deviation from the Mott relationship through correlated electron states. Raman spectra of the $(PbSe)_{1+\delta}(VSe_2)_1$ material show the emergence of additional peaks below the CDW transition temperature associated with VSe_2 material. Temperature-dependent in-plane X-ray diffraction (XRD) spectra show a change in the in-plane thermal expansion of VSe_2 in $(PbSe)_{1+\delta}(VSe_2)_1$ due to lattice distortion. The increase in the power factor and decrease in the resistivity due to CDW suggest a potential mechanism for enhancing the thermoelectric performance at the low temperature region.

KEYWORDS: Charge density wave, transition-metal dichalcogenide, thermoelectrics, thermoelectricity, energy conversion, many body

■ INTRODUCTION

Since the 1950s, many researchers have tried to improve the thermoelectric efficiency of materials using various strategies including asymmetric density of states in low dimensional materials, 1,2 engineering materials and nanostructures with low lattice thermal conductivity, 3,4 and distortion of the density of states and creating resonant levels in the materials. 5,6 It should be noted that, while there are relatively good thermoelectric materials (i.e., ZT ~ 1) at room temperature and elevated temperatures (e.g., 800-1000 °C), there are currently no efficient thermoelectric materials at low temperatures. The phenomenon presented here can potentially provide a new mechanism for increased thermoelectric performance at low temperatures that deviates from the standard Mott relationship through the creation of correlated electron states. Several transition-metal dichalcogenides (TMDCs) exhibit charge density wave (CDW) transitions at low temperatures.⁷ Below the transition temperature, $T_{\rm CDW}$, the atomic lattice forms a periodic structural distortion, which creates a condensed ground state of electrons and a gap in the Fermi surface. 7,8 As a result, the electrical resistivity usually increases below $T_{\rm CDW}$. Under applied electrostatic gate fields, the CDW can become unpinned from impurities and slide with respect to the lattice. The sliding CDW can then contribute to the electron transport, adding to the single-particle conductance contribution. 9,10 This collective conductance caused by the CDW sliding motion can be modulated with an applied gate voltage up to 2 orders of magnitude higher than the single-particle conductance. 11

Received: July 13, 2020 Revised: October 9, 2020

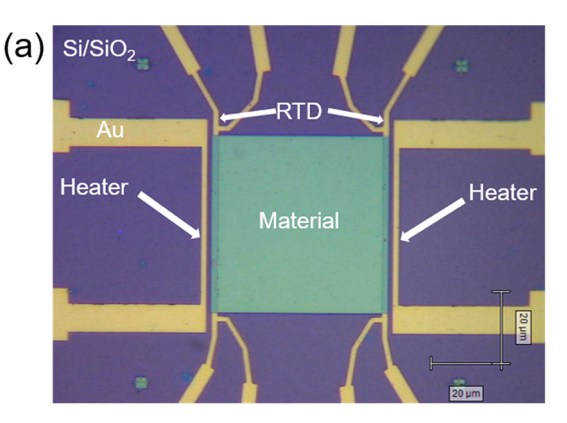


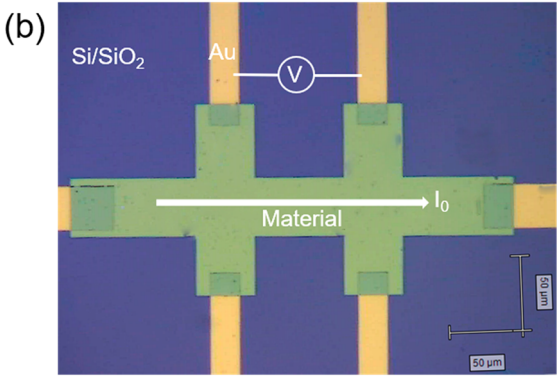
In TiSe₂ and VSe₂, the resistivity increases due to the CDW transition and the transition temperature has been found to depend on both the applied pressure and layer thickness, ^{12–15} which tune the interlayer interaction. VSe2 is composed of hexagonally stacked Se-V-Se sheets with interlayer van der Waals bonding¹⁴ and has a CDW transition temperature near 100 K. 16 Recent work by the Johnson group has shown that the transition temperature can be tuned by changing the PbSe separation thickness (m) or the VSe₂ layer thickness (n) in $[(PbSe)_{1+\delta}]_m(VSe_2)_n$ heterostructures. The in-plane resistivity increase below $T_{\rm CDW}$ is found to be most pronounced in $[(PbSe)_{1+\delta}]_1(VSe_2)_1$ structures. The in-plane resistivity increases below T_{CDW} in $[(PbSe)_{1+\delta}]_m(VSe_2)_1$ structures are much more pronounced than observed in bulk VSe₂. ^{17,18} To our knowledge, no thermoelectric measurements have been performed on this interesting new materials system. The crossplane thermal conductivity of semiconducting layered heterostructures has been found to be ultralow ($\kappa \sim 0.05 \text{ W/m} \cdot \text{K}$). making them promising candidates for thermoelectric applications.3 The in-plane lattice thermal conductivity of these materials has also been found to be quite low ($\kappa_l \sim 0.4$ W/m·K) according to the measurements with the use of suspended microdevices. ^{19,20} Both the in-plane and cross-plane thermal conductivity measurements were done on semiconducting systems, where the electronic contribution to the thermal conductivity (κ_e) is negligible. In comparison, κ_e can be significant in $[(PbSe)_{1+\delta}]_m(VSe_2)_n$ in the normal metallic state above $T_{\rm CDW}$ and can be calculated from the measured electrical conductivity using the Wiedemann-Franz law. 21,22 However, the Wiedemann-Franz law does not necessarily hold true for CDW systems²³ due to electron-electron interactions as well as the collective conductance associated with the sliding motion of the CDW from electron-phonon coupling. 24-28 Previous thermal conductivity measurements across the CDW transition have shown an unusual peak in thermal conductivity at the CDW transition, which was explained by an additional contribution from low frequency phasons. 29,30

Here, we explore the thermoelectric transport properties of $(PbSe)_{1+\delta}(VSe_2)_1$ and $(PbSe)_{1+\delta}(VSe_2)_2$ heterostructures both above and below the charge density wave transition temperature observed in the $(PbSe)_{1+\delta}(VSe_2)_1$ heterostructure. These measurements entail both in-plane electrical conductivity and Seebeck coefficient measurements as a function of temperature. We also measure the temperature dependence of the Raman spectra of these materials in order to substantiate that a structural change occurs at the CDW transition. Specular and in-plane diffraction scans were measured. The room temperature structures of both compounds and the temperature dependence of the lattice parameters of $(PbSe)_{1+\delta}(VSe_2)_1$ were determined from the diffraction patterns.

RESULTS AND DISCUSSION

Figure 1 shows optical microscope images of the sample used to measure the in-plane Seebeck coefficient and electrical resistivity, via a 4-point resistivity measurement which eliminates the effect of contact resistance. Here, the Seebeck coefficient was measured by small microfabricated heaters and thermometers fabricated using electron beam lithography. The $[({\rm PbSe})_{1+\delta}({\rm VSe_2})_n]$ films, approximately 50 nm thick, were deposited in lithographically defined windows approximately 50 $\mu{\rm m}\times$ 50 $\mu{\rm m}$ in size followed by a lift-off process. 4,31 We measured the temperature dependence of the Raman spectra in





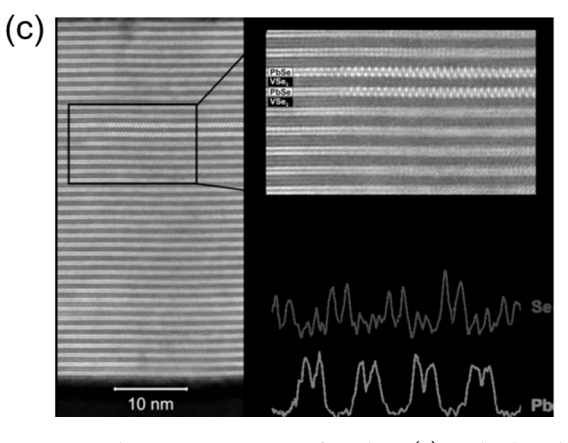
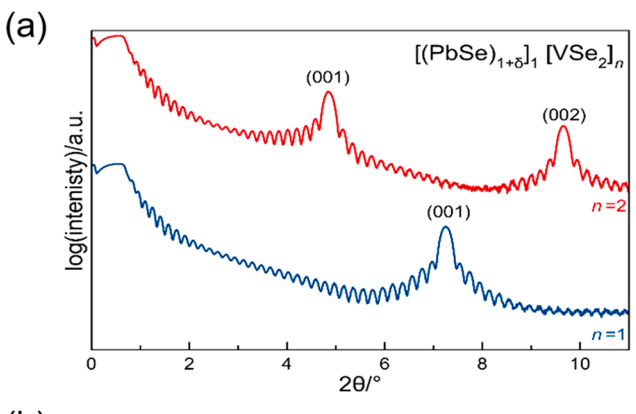


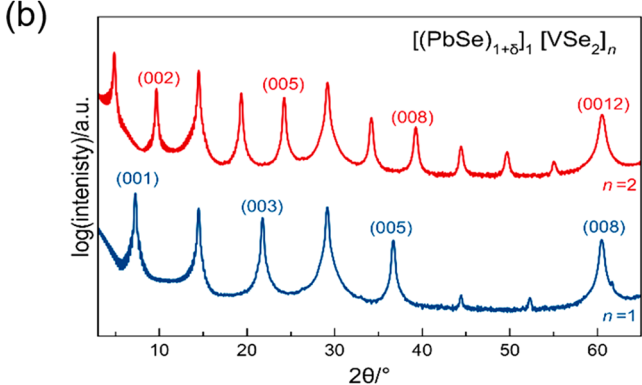
Figure 1. Optical microscope image of in-plane (a) Seebeck and (b) resistivity measurements of the $(PbSe)_{1+\delta}(VSe_2)_n$ films. (c) HAADF-STEM image of the $(PbSe)_{1+\delta}(VSe_2)_1$ heterostructure film.

an optical cryostat. The $(PbSe)_{1+\delta}(VSe_2)_n$ films used in this study were formed via the self-assembly of various precursors by physical vapor deposition (PVD) of elemental sources in a home-built high vacuum chamber ($<5 \times 10^{-7}$ Torr). Pb and V were deposited by electron beam evaporation, and Se was deposited with a Knudsen effusion cell. Each constituent element was deposited sequentially to form the layered precursors that matched the chemical component ratios of each desired target structure. The distance between the source and substrates was approximately 1 m, and evaporation rates were maintained below 1 Å/s. Films were deposited on both unpatterned substrates (for structural characterization) and patterned substrates (for in-plane transport measurements). Calibrated deposition parameters have been previously reported for the $(PbSe)_{1+\delta}(VSe_2)_n$ compounds. The films were crystallized into the layered structures after the deposition in an inert N₂ environment by heating to 250 °C for 60 min.

The thickness of as-deposited films was 50 nm. Figure 1c shows the high-angle annular dark-field scanning transmission electron microscopy (HAADF-STEM) measurement of the (PbSe)_{1+ δ}(VSe₂)₁ heterostructure film. In the figure, alternating PbSe and VSe₂ layers are clearly distinct from each other. Here, the PbSe layers are considerably brighter than the VSe₂ layers.

X-ray diffraction characterization of the $(PbSe)_{1+\delta}(VSe_2)_n$ heterostructures was performed after annealing the precursors. Figure 2 contains the X-ray reflectivity of two samples





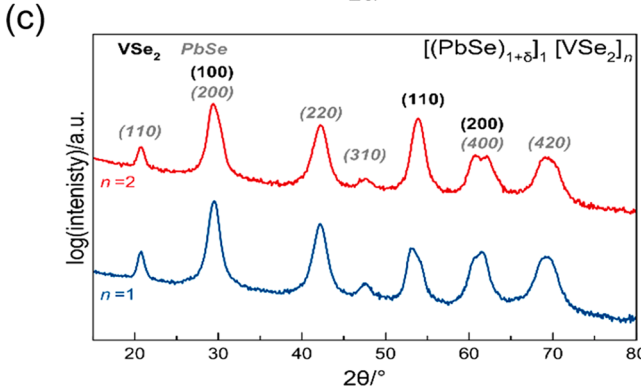


Figure 2. (a) Low angle X-ray reflectivity (XRR) patterns, (b) specular X-ray diffraction patterns, and (c) grazing incidence in-plane X-ray diffraction patterns for the samples investigated in this study. The corresponding Miller indices are also labeled for each material.

investigated in this work. The spectra contain Kiessig fringes below the first-order Bragg reflections from the heterostructures and Laue oscillations after the first-order Bragg reflection from the finite number of unit cells in the films. The observation of fringes beyond 10° indicates that the films have less than an angstrom of roughness within the coherence of the

X-ray source. All of the maxima in the specular diffraction patterns can be indexed as 00l planes, indicating that the samples are crystallographically aligned with the substrate. The c-axis lattice parameters calculated from the patterns (c = 12.23(1) Å and 18.31(1) Å for $(PbSe)_{1+\delta}(VSe_2)_1$ and $(PbSe)_{1+\delta}(VSe_2)_2$, respectively) agree with those previously reported. The maxima in the grazing incident in-plane diffraction patterns can all be indexed as hk0 reflections of either PbSe or VSe₂ planes, confirming the crystallographic alignment of the crystals with the substrate. The in-plane lattice parameters are consistent with those previously reported. The lengths of the a-axis of PbSe are 6.06(1) Å for both materials, and the a-axis lengths of VSe₂ are 3.43(1) Å and 3.40(1) Å for $(PbSe)_{1+\delta}(VSe_2)_1$ and $(PbSe)_{1+\delta}(VSe_2)_2$, respectively. Figure 2c shows that the PbSe pattern contains 110 and 310 reflections that are forbidden in the rock salt structure, indicating that the crystal structure, while still cubic, has distorted slightly from that of the bulk. Lattice parameters were determined from in-plane X-ray diffraction (XRD) spectra of the $(PbSe)_{1+\delta}(VSe_2)_1$ compound collected as a function of temperature at the Advanced Photon Source (APS) and are plotted as a function of temperature in Figure S1 of the Supporting Information. The slope of the change in the inplane lattice parameter as a function of temperature of VSe₂ changes its sign at ~125 K, indicating that VSe₂ layers undergo a structural transition at low temperature while the PbSe does

Figure 3 shows a comparison of the in-plane electrical resistivity and Seebeck coefficient plotted as a function of temperature over the range of 77-300 K for both the $(PbSe)_{1+\delta}(VSe_2)_1$ and $(PbSe)_{1+\delta}(VSe_2)_2$ heterostructures. For the $(PbSe)_{1+\delta}(VSe_2)_1$ material, the electrical resistivity shows a minimum around T = 140 K, while the $(PbSe)_{1+\delta}(VSe_2)_2$ material shows a linear monotonically increasing resistivity with temperature over the entire temperature range as expected for a metal. These results are consistent with our previous measurement of charge density waves in this material system, where we reported a CDW transition around 140 K for the 1:1 material and not the 1:2 material. The Seebeck coefficient plotted in Figure 3b shows a large abrupt increase from 10.6 to 19.7 μ V/K (increases by 85%) for the $(PbSe)_{1+\delta}(VSe_2)_1$ film when the temperature is lowered from 150 to 136 K, while the resistivity actually decreases from 3.768 to 3.765 μ Ohm·m over the same temperature range (shown in the inset in Figure 3a). $(PbSe)_{1+\delta}(VSe_2)_2$ does not show this behavior and has a relatively low Seebeck coefficient $(3.4 \,\mu\text{V/K})$. Tani et al. reported a similar abrupt change in the Seebeck coefficient of 1T-TaS2 around 210 K due to a CDW transition. However, this behavior was observed only in one out of a total of six samples. 32,33 Bhatt et al. and Huang et al. reported Seebeck coefficient measurements through the CDW transition of TiSe2-x, which resulted in gradual changes in the resistivity and Seebeck coefficient. However, the suppression of the CDW transition actually improved the thermoelectric performance in their samples. 34,35 Naik and Rastogi studied 2H-NbSe₂ with and without Ga-intercalation and found that resistivity shows a kink and the Seebeck coefficient has broad maximum around 35 K for a single crystalline structure and that the CDW effect is quenched with Ga-intercalation.³⁶ Compared to a previous thermoelectric study on other CDW materials, the enhancement in the Seebeck coefficient and the power factor observed in our $(PbSe)_{1+\delta}(VSe_2)_1$ heterostructures results from two reasons. The first reason is that reducing

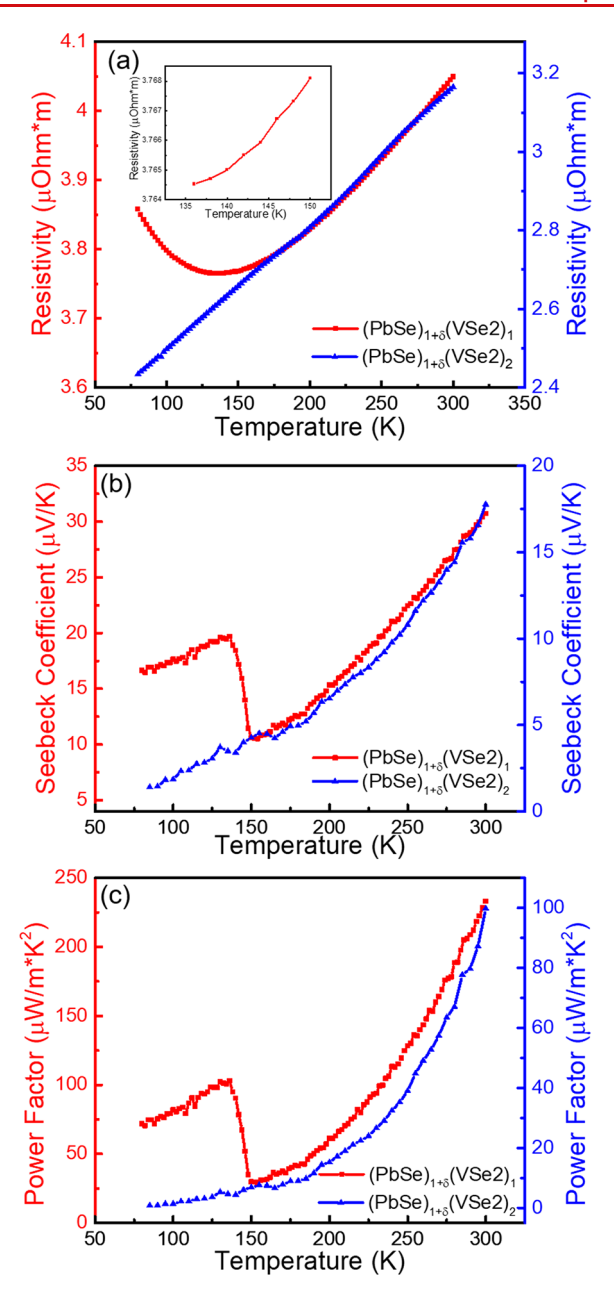


Figure 3. (a) Electrical resistivity, (b) Seebeck coefficient, and (c) power factor of $(PbSe)_{1+\delta}(VSe_2)_n$ films plotted as a function of temperature. The inset in Figure 3a shows the change in resistivity over the temperature range during which the Seebeck coefficient exhibits a sudden jump for the $(PbSe)_{1+\delta}(VSe_2)_1$ material.

the dimensions of the VSe_2 component to the monolayer limit will enhance the CDW order and Fermi-surface nesting through correlated electron states. Research by Feng et al. shows that their density functional theory (DFT) calculation overestimates the bandwidth of near- $E_{\rm F}$ energy states compared to experimentally observed values by a factor of 1.4. The discrepancy is attributed to electron–electron interaction from V 3d orbitals that has not been included in the DFT. Duvjir et al. demonstrate strong CDW order and perfect Fermi-surface nesting due to enhanced electron–electron correlations in monolayer VSe₂. Recond, the heterointerface between the VSe₂ and PbSe layers also plays an important role in electronic reconstruction. A metal–insulator transition was observed around 135 K in a monolayer

VSe₂/bilayer graphene system, which is caused by heterointerfacial coupling between VSe2 and graphene layers, such as interlayer charge transfer and hybridization.²⁷ We observe only enhanced thermoelectric performance in $(PbSe)_{1+\delta}(VSe_2)_1$, because the CDW is observed only when there is a monolayer VSe_2 sandwiched by two PbSe layers. In the $(PbSe)_{1+\delta}(VSe_2)_2$ heterostructure the CDW is similar to that observed in bulk VSe₂. Above the CDW transition temperature, the two materials (1:1 and 1:2 heterostructures) studied here show very similar behaviors with the VSe₂ in the metallic state. We observed the same Seebeck and resistivity temperaturedependent profiles on several different samples. In order to characterize the thermoelectric performance of those materials, power factors as a function of temperature have been calculated and are shown in Figure 3c. The power factor of the $(PbSe)_{1+\delta}(VSe_2)_1$ film changes from 29.8 $\mu W/m \cdot K^2$ above to 102.9 μ W/m·K² below the CDW transition, corresponding to a 245% increase in the power factor. This large enhancement in the power factor of the $(PbSe)_{1+\delta}(VSe_2)_1$ film originates from a sudden jump in the Seebeck coefficient and slight decrease in resistivity. The power factor of $(PbSe)_{1+\delta}(VSe_2)_2$ is 4.4 $\mu W/m \cdot K^2$ at the transition temperature. The ratio of power factors between these two materials increases from 7 above to more than 23 below the CDW. At 80 K the ratio of the power factors has increased to 90 [the $(PbSe)_{1+\delta}(VSe_2)_2$ film has a power factor 0.8 $\mu W/m \cdot K^2$, while $(PbSe)_{1+\delta}(VSe_2)_1$ has a power factor of 72 $\mu W/m \cdot K^2$]. We would like to emphasize that the 1:2 heterostructures (i.e., $(PbSe)_{1+\delta}(VSe_2)_2$) did not show a CDW transition, and we believe this phenomenon is unique to the monolayer structure. Hite et al. found that the temperature-dependent mobility of the $(PbSe)_{1+\delta}(VSe_2)_1$ heterostructure decreases from 1.1 to 0.6 cm²/V·s when the temperature decreases from 300 to 120 K. When the temperature is below the CDW transition temperature, the mobility starts to increase and reaches 1.6 cm^2/V ·s when $T = 10 \text{ K.}^{17} \text{ A}$ unique feature that we have observed is that the Seebeck coefficient increases abruptly below the transition temperature while the resistivity decreases slightly. This behavior is rather unusual compared to the general trend that has been observed in other material systems. This unique trend has led to a large increase of the Seebeck coefficient and the power factor right below the transition temperature. The unusual combination of increasing Seebeck and reduced resistivity is apparently related to the presence of electron-electron correlation. Although the values of the Seebeck coefficient and the power factor of our materials are low and lack commercial interest at this point of development, the enhancement percentages reported here are quite high (86% in Seebeck and 245% in power factor). Our findings suggest a potential enhancement mechanism for thermoelectric performance worthy of further investigation in future thermoelectric materials design.

Figure 4 shows the Seebeck coefficient over temperature (S/T) as a function of one over conductivity ($1/\sigma$) for (PbSe)_{1+ δ}(VSe₂)_{1,2} heterostructures. Under the assumption of weak electron–electron interaction, the Mott relation gives the Seebeck coefficient of a metallic system as

$$S = -\frac{\pi^2 k_B^2}{3} \frac{T}{e} \frac{d\sigma}{\sigma} dE \Big|_{E_F}$$
 (1)

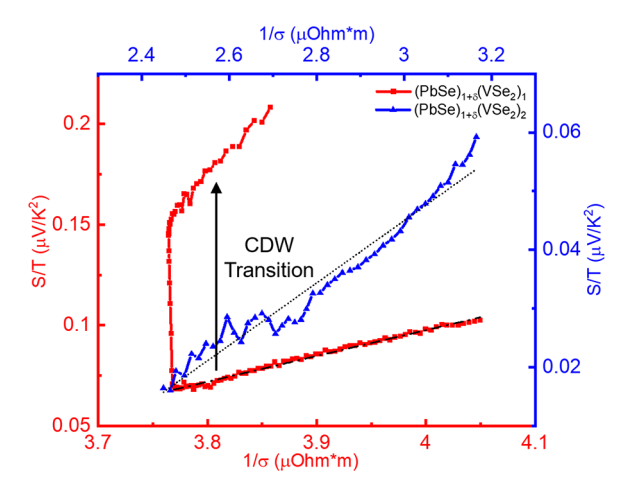


Figure 4. S/T vs $1/\sigma$ of $(PbSe)_{1+\delta}(VSe_2)_{1,2}$ heterostructure materials. The dashed and dotted black lines are the linear fitted regions of $(PbSe)_{1+\delta}(VSe_2)_1$ and $(PbSe)_{1+\delta}(VSe_2)_2$ films, respectively.

where S is the Seebeck coefficient, $k_{\rm B}$ is the Boltzmann constant, T is the absolute temperature, e is electron charge, and σ is electrical conductivity. Equation 1 can be rewritten as

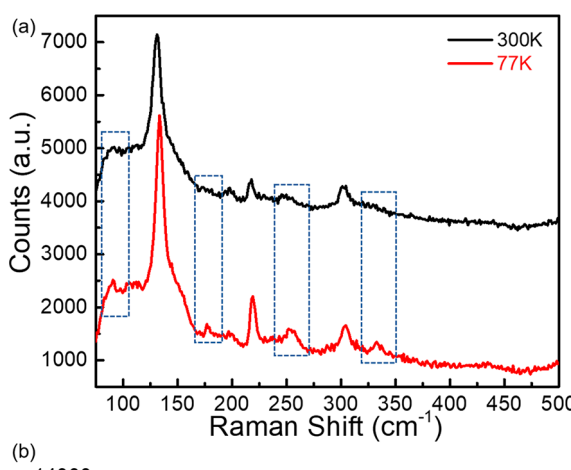
$$\frac{S}{T} = \left(-\frac{\pi^2}{3} \frac{k_B^2}{e} \frac{d\sigma}{dE} |_{E_F} \right) \frac{1}{\sigma}$$
(2)

Figure 4 contains a plot of S/T vs $1/\sigma$ for both $(PbSe)_{1+\delta}(VSe_2)_1$ and $(PbSe)_{1+\delta}(VSe_2)_2$. In $(PbSe)_{1+\delta}(VSe_2)_2$, the S/T versus $1/\sigma$ relationship is linear over the entire measured temperature range (80-300 K) as indicated by a black dotted line, indicating that $\frac{d\sigma}{dE}|_{E_{\rm F}}$ is roughly constant over this range. In addition, $d\sigma/dE$ can be written as $(d\sigma/dn)(dn/dE) = e\mu(dn/dE)$, where e is electron charge, μ is the mobility, and dn/dE is proportional to the density of states. For (PbSe)_{1+ δ}(VSe₂)₁, the S/T vs 1/ σ is similarly linear between room temperature and the CDW transition temperature of ~140 K, where the Mott relation is expected to be satisfied. Below 140 K there is a distinct change in behavior as the structure undergoes a structural distortion. The Mott relation is no longer valid below the CDW transition temperature because the conduction electron movements are highly correlated and no longer independent, and because the CDW transition is accompanied by a gap opening in the electronic structure to make the system nonmetallic.

Mavrokefalos et al. showed that the in-plane thermal conductivities of $[(PbSe)_{0.99}]_x(WSe_2)_x$ with x=2, 3, 4 are around 0.5 W/m·K at room temperature and are insensitive to interface density. ^{19,20} For our $(PbSe)_{1+\delta}(VSe_2)_1$ and $(PbSe)_{1+\delta}(VSe_2)_2$ heterostructures, the thermal conductivity could contain an appreciable electrical contribution since the VSe₂ layers are metallic. Figure S2 shows the estimated electrical contribution of the in-plane thermal conductivities κ_{\parallel} of these two heterostructures based on the Wiedemann–Franz (WF) law using temperature-dependent resistivities data. Both heterostructures exhibit monotonically decreasing behavior as temperature decreases. At each temperature, the κ_{\parallel} of $(PbSe)_{1+\delta}(VSe_2)_2$ is higher than that of $(PbSe)_{1+\delta}(VSe_2)_1$, due to the higher percentage of VSe_2 layers in the $(PbSe)_{1+\delta}(VSe_2)_2$ material. However, it should be noted that, for $(PbSe)_{1+\delta}(VSe_2)_1$ material, the WF law may not hold true

when the temperature is below the CDW transition temperature.

In order to further probe the presence of structural change with respect to temperature, the in-plane diffraction patterns of the $(PbSe)_{1+\delta}(VSe_2)_1$ heterostructure were measured at several different temperatures (Advanced Photon Source, Beamline 33-BM). Figure S1a plots the in-plane lattice parameters of VSe₂ and PbSe as a function of temperature. A local minimum of lattice parameter of VSe₂ is observed when the temperature is around the CDW phase transition. The thermal expansion coefficient of VSe₂ in (PbSe)_{1+ δ}(VSe₂)₁ is about 10×10^{-6} /K between 140 to 300 K. This is approximately a factor of 2 smaller than the linear thermal expansion coefficient of bulk VSe_2 (18.6 × 10⁻⁶/K). However, below 140 K the thermal expansion coefficient is negative, at approximately $-30 \times$ 10^{-6} /K. The thermal expansion coefficient of the PbSe layer remains constant over the entire temperature range and is within a factor of 2 found for bulk PbSe. The change in the thermal expansion coefficient of the VSe₂ constituent is consistent with a structural change occurring at ~140 K. Raman spectra of the $(PbSe)_{1+\delta}(VSe_2)_1$ and $(PbSe)_{1+\delta}(VSe_2)_2$ heterostructures taken at 77 and 300 K, shown in Figure 5, also suggest a structural change in the VSe2 layer of $(PbSe)_{1+\delta}(VSe_2)_1$ as temperature is decreased. For the 1:1 heterostructure material, we see the emergence of several additional peaks in the Raman spectra at temperatures at 77 K, which is consistent with a transition to a lower symmetry



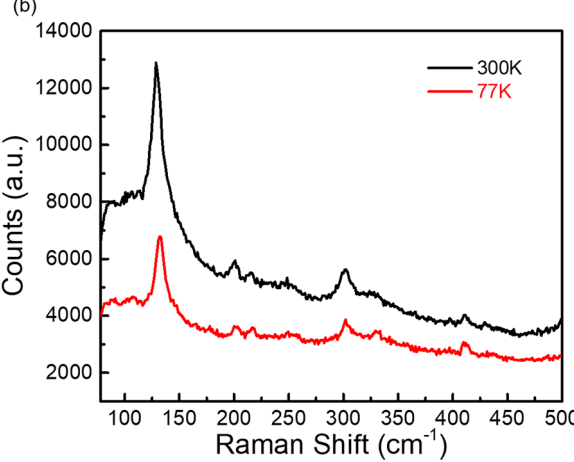


Figure 5. Raman spectra of (a) $(PbSe)_{1+\delta}(VSe_2)_1$ and (b) $(PbSe)_{1+\delta}(VSe_2)_2$ heterostructures measured at room temperature (300 K) and 77 K.

lattice structure associated with the CDW of the VSe₂ constituent. As a control, the Raman spectra of the $(PbSe)_{1+\delta}(VSe_2)_2$ heterostructure do not show any temperature dependence. Previously, Balandin and co-workers reported similar changes in the temperature dependence of the Raman spectra of TiSe2 corresponding to a CDW transition. 12 It should be noted that bulk VSe2 exhibits a CDW transition with a much smaller change in resistivity above and below the CDW temperature. In $(PbSe)_{1+\delta}(VSe_2)_1$ and $(PbSe)_{1+\delta}(VSe_2)_2$ the VSe_2 layers have one or two adjacent PbSe layers rather than adjacent VSe₂ layers, and there will be charge transfer between the PbSe and VSe2 layers, Both of these differences will change the CDW transition behavior of the VSe₂ layers relative to bulk VSe₂. The striking difference in behavior between the (PbSe)_{1+ δ}(VSe₂)₁ and (PbSe)_{1+ δ}(VSe₂)₂ materials is consistent with our previous measurements.

CONCLUSION

In conclusion, we report the temperature-dependent thermoelectric properties of $(PbSe)_{1+\delta}(VSe_2)_1$ and $(PbSe)_{1+\delta}(VSe_2)_2$ heterostructure materials. The $(PbSe)_{1+\delta}(VSe_2)_1$ material shows an increased Seebeck coefficient from 10.6 to 19.7 $\mu V/K$ (85% increase) and increased power factor from 29.8 to 102.9 μ W/m·K² (245% increase) before and after the CDW phase transition, while the change in resistivity over the same temperature range is negligible. The (PbSe)_{1+ δ}(VSe₂)₂ material shows monotonically increasing values of the transport properties with temperature and lower values than those of the $(PbSe)_{1+\delta}(VSe_2)_1$ film. Above the CDW transition temperature, the S/T vs $1/\sigma$ relationship is linear for both heterostructures in accordance with the Mott equation, which is valid for metals with weak electron-electron interactions. However, non-Mott behavior appears below the CDW transition for the $(PbSe)_{1+\delta}(VSe_2)_1$ material, resulting from the highly correlated conduction of electrons. Furthermore, temperature-dependent in-plane XRD and Raman spectra indicate unique structural changes for the $(PbSe)_{1+\delta}(VSe_2)_1$ heterostructure film. The mechanism underlying these results may be used to provide a new approach for enhancing the thermoelectric performances of materials at low temperatures.

ASSOCIATED CONTENT

Supporting Information

The Supporting Information is available free of charge at https://pubs.acs.org/doi/10.1021/acs.nanolett.0c02882.

Temperature-dependent basal plane area of $(PbSe)_{1+\delta}(VSe_2)_1$ measured by in-plane X-ray diffraction; estimated thermal conductivities of $(PbSe)_{1+\delta}(VSe_2)_1$ and $(PbSe)_{1+\delta}(VSe_2)_2$ materials based on the Wiedemann–Franz (WF) law (PDF)

AUTHOR INFORMATION

Corresponding Author

Stephen B. Cronin — Ming Hsieh Department of Electrical Engineering, Department of Chemistry, and Department of Physics and Astronomy, University of Southern California, Los Angeles, California 90089, United States; oocid.org/0000-0001-9153-7687; Email: scronin@usc.edu

Authors

Yu Wang — Mork Family Department of Chemical Engineering and Materials Science, University of Southern California, Los Angeles, California 90089, United States; o orcid.org/0000-0002-0307-1301

Danielle M. Hamann – Department of Chemistry, University of Oregon, Eugene, Oregon 97403-1253, United States;
orcid.org/0000-0002-9262-1060

Dmitri Leo M. Cordova — Department of Chemistry, University of Oregon, Eugene, Oregon 97403-1253, United States;
orcid.org/0000-0002-7527-8950

Jihan Chen — Ming Hsieh Department of Electrical Engineering, University of Southern California, Los Angeles, California 90089, United States; ⊚ orcid.org/0000-0001-7065-8287

Bo Wang — Department of Physics and Astronomy, University of Southern California, Los Angeles, California 90089, United States; Occid.org/0000-0001-7089-6672

Lang Shen – Mork Family Department of Chemical Engineering and Materials Science, University of Southern California, Los Angeles, California 90089, United States

Zhi Cai – Mork Family Department of Chemical Engineering and Materials Science, University of Southern California, Los Angeles, California 90089, United States

Haotian Shi – Department of Chemistry, University of Southern California, Los Angeles, California 90089, United States

Evguenia Karapetrova — Advanced Photon Source, Argonne National Laboratory, Lemont, Illinois 60439, United States

Indu Aravind — Department of Physics and Astronomy, University of Southern California, Los Angeles, California 90089, United States

Li Shi — Department of Mechanical Engineering and Texas Materials Institute, University of Texas at Austin, Austin, Texas 78712, United States; oorcid.org/0000-0002-5401-6839

David C. Johnson – Department of Chemistry, University of Oregon, Eugene, Oregon 97403-1253, United States;
orcid.org/0000-0002-1118-0997

Complete contact information is available at: https://pubs.acs.org/10.1021/acs.nanolett.0c02882

Note

The authors declare no competing financial interest.

■ ACKNOWLEDGMENTS

This research was supported by the Department of Energy (DOE) [award nos. DE-FG02-07ER46376 (Y.W.), DE-FG02-07ER46377 (L.S.)] and by the NSF [award nos. CBET-2012845 (Z.C.) and CBET-1905357 (J.C.)]. This material is based upon work supported by the National Science Foundation Graduate Research Fellowship Program under grant no. 1309047. Any opinions, findings, and conclusions or recommendations expressed in this material are those of the author(s) and do not necessarily reflect the views of the National Science Foundation. The authors acknowledge support from the National Science Foundation under grant DMR-1710214.

REFERENCES

(1) Hicks, L. D.; Dresselhaus, M. S. Use of Quantum-Well Superlattices to Obtain a High Figure of Merit from Nonconventional Thermoelectric Materials. MRS Online Proc. Libr. 1993, 326, 413. (2) Hicks, L. D.; Harman, T. C.; Sun, X.; Dresselhaus, M. S. Experimental Study of the Effect of Quantum-Well Structures on the Thermoelectric Figure of Merit. Phys. Rev. B: Condens. Matter Mater. Phys. 1996, 53, 10493–10496.

- (3) Chiritescu, C.; Cahill, D. G.; Nguyen, N.; Johnson, D.; Bodapati, A.; Keblinski, P.; Zschack, P. Ultralow Thermal Conductivity in Disordered, Layered WSe, Crystals. *Science* **2007**, *315*, 351.
- (4) Li, Z.; Bauers, S. R.; Poudel, N.; Hamann, D.; Wang, X.; Choi, D. S.; Esfarjani, K.; Shi, L.; Johnson, D. C.; Cronin, S. B. Cross-Plane Seebeck Coefficient Measurement of Misfit Layered Compounds (SnSe)n(TiSe₂)n (n = 1,3,4,5). *Nano Lett.* **2017**, *17*, 1978–1986.
- (5) Heremans, J. P.; Jovovic, V.; Toberer, E. S.; Saramat, A.; Kurosaki, K.; Charoenphakdee, A.; Yamanaka, S.; Snyder, G. J. Enhancement of Thermoelectric Efficiency in PbTe by Distortion of the Electronic Density of States. *Science* **2008**, *321*, 554.
- (6) Heremans, J. P.; Wiendlocha, B.; Chamoire, A. M. Resonant Levels in Bulk Thermoelectric Semiconductors. *Energy Environ. Sci.* **2012**, *5*, 5510–5530.
- (7) Wilson, J. A.; Di Salvo, F. J.; Mahajan, S. Charge-Density Waves in Metallic, Layered, Transition-Metal Dichalcogenides. *Phys. Rev. Lett.* **1974**, 32, 882–885.
- (8) Rossnagel, K. On the Origin of Charge-Density Waves in Select Layered Transition-Metal Dichalcogenides. *J. Phys.: Condens. Matter* **2011**, 23, 213001.
- (9) Thorne, R. E. Charge-Density-Wave Conductors. *Phys. Today* **1996**, 49, 42–47.
- (10) Grüner, G. The dynamics of charge-density waves. *Rev. Mod. Phys.* **1988**, *60*, 1129–1181.
- (11) Adelman, T. L.; Zaitsev-Zotov, S. V.; Thorne, R. E. Field-Effect Modulation of Charge-Density-Wave Transport in NbSe₃ and TaS₃. *Phys. Rev. Lett.* **1995**, *74*, 5264–5267.
- (12) Goli, P.; Khan, J.; Wickramaratne, D.; Lake, R. K.; Balandin, A. A. Charge Density Waves in Exfoliated Films of van der Waals Materials: Evolution of Raman Spectrum in TiSe₂. *Nano Lett.* **2012**, 12, 5941–5945.
- (13) Kusmartseva, A. F.; Sipos, B.; Berger, H.; Forró, L.; Tutiš, E. Pressure Induced Superconductivity in Pristine 1T-TiSe₂. *Phys. Rev. Lett.* **2009**, *103*, 236401.
- (14) Yang, J.; Wang, W.; Liu, Y.; Du, H.; Ning, W.; Zheng, G.; Jin, C.; Han, Y.; Wang, N.; Yang, Z.; Tian, M.; Zhang, Y. Thickness Dependence of the Charge-Density-Wave Transition Temperature in VSe₂. Appl. Phys. Lett. **2014**, 105, 063109.
- (15) Friend, R. H.; Jérome, D.; Schleich, D. M.; Molinié, P. Pressure Enhancement of Charge Density Wave Formation in VSe₂; The Role of Coulomb Correlations. *Solid State Commun.* **1978**, *27*, 169–173.
- (16) Eaglesham, D. J.; Withers, R. L.; Bird, D. M. Charge-Density-Wave Transitions in 1T-VSe₂. *J. Phys. C: Solid State Phys.* **1986**, *19*, 359.
- (17) Hite, O. K.; Falmbigl, M.; Alemayehu, M. B.; Esters, M.; Wood, S. R.; Johnson, D. C. Charge Density Wave Transition in $(PbSe)_{1+\delta}(VSe_2)_n$ Compounds with n=1, 2, and 3. *Chem. Mater.* **2017**, 29, 5646–5653.
- (18) Cordova, D. L. M.; Fender, S. S.; Kam, T. M.; Seyd, J.; Albrecht, M.; Lu, P.; Fischer, R.; Johnson, D. C. Designed Synthesis and Structure–Property Relationships of Kinetically Stable $[(PbSe)_{1+\delta}]_m(VSe_2)_1$ (m = 1, 2, 3, 4) Heterostructures. *Chem. Mater.* **2019**, 31, 8473–8483.
- (19) Mavrokefalos, A.; Lin, Q.; Beekman, M.; Seol, J. H.; Lee, Y. J.; Kong, H.; Pettes, M. T.; Johnson, D. C.; Shi, L. In-Plane Thermal and Thermoelectric Properties of Misfit-Layered [(PbSe)_{0.99}]_x(WSe₂)_x Superlattice Thin Films. *Appl. Phys. Lett.* **2010**, *96*, 181908.
- (20) Mavrokefalos, A.; Nguyen, N. T.; Pettes, M. T.; Johnson, D. C.; Shi, L. In-Plane Thermal Conductivity of Disordered Layered WSe₂ and (W)_x(WSe₂)_y Superlattice Films. *Appl. Phys. Lett.* **2007**, *91*, 171912.
- (21) Westover, R. D.; Atkins, R. A.; Ditto, J. J.; Johnson, D. C. Synthesis of $[(SnSe)_{1.16-1.09}]_1[(Nb_xMo_{1-x}) Se_2]_1$ Ferecrystal Alloys. *Chem. Mater.* **2014**, *26*, 3443–3449.
- (22) Falmbigl, M.; Fiedler, A.; Atkins, R. E.; Fischer, S. F.; Johnson, D. C. Suppressing a Charge Density Wave by Changing Dimensionality in the Ferecrystalline Compounds ($[SnSe]_{1.15}$)₁(VSe_2)_n with n = 1, 2, 3, 4. Nano Lett. **2015**, 15, 943–948.

- (23) Mahajan, R.; Barkeshli, M.; Hartnoll, S. A. Non-Fermi Liquids and the Wiedemann-Franz Law. *Phys. Rev. B: Condens. Matter Mater. Phys.* **2013**, 88, 125107.
- (24) Bayard, M.; Sienko, M. Anomalous Electrical and Magnetic Properties of Vanadium Diselenide. *J. Solid State Chem.* **1976**, *19*, 325–329
- (25) Xu, K.; Chen, P.; Li, X.; Wu, C.; Guo, Y.; Zhao, J.; Wu, X.; Xie, Y. Ultrathin Nanosheets of Vanadium Diselenide: A Metallic Two-Dimensional Material with Ferromagnetic Charge-Density-Wave Behavior. *Angew. Chem., Int. Ed.* **2013**, *52*, 10477–10481.
- (26) Feng, J.; Biswas, D.; Rajan, A.; Watson, M. D.; Mazzola, F.; Clark, O. J.; Underwood, K.; Markovic, I.; McLaren, M.; Hunter, A.; Burn, D. M.; Duffy, L. B.; Barua, S.; Balakrishnan, G.; Bertran, F.; Le Fevre, P.; Kim, T. K.; van der Laan, G.; Hesjedal, T.; Wahl, P.; King, P. D. C. Electronic Structure and Enhanced Charge-Density Wave Order of Monolayer VSe₂. *Nano Lett.* **2018**, *18*, 4493–4499.
- (27) Duvjir, G.; Choi, B. K.; Jang, I.; Ulstrup, S.; Kang, S.; Thi Ly, T.; Kim, S.; Choi, Y. H.; Jozwiak, C.; Bostwick, A.; Rotenberg, E.; Park, J. G.; Sankar, R.; Kim, K. S.; Kim, J.; Chang, Y. J. Emergence of a Metal-Insulator Transition and High-Temperature Charge-Density Waves in VSe2 at the Monolayer Limit. *Nano Lett.* **2018**, *18*, 5432–5438.
- (28) Jang, I.; Duvjir, G.; Choi, B. K.; Kim, J.; Chang, Y. J.; Kim, K.-S. Universal renormalization group flow toward perfect Fermi-surface nesting driven by enhanced electron-electron correlations in monolayer vanadium diselenide. *Phys. Rev. B: Condens. Matter Mater. Phys.* **2019**, *99*, 1.
- (29) Harper, J. M. E.; Geballe, T. H.; DiSalvo, F. J. Thermal Properties of Layered Transition-Metal Dichalcogenides at Charge-Density-Wave Transitions. *Phys. Rev. B* **1977**, *15*, 2943–2951.
- (30) Smontara, A.; Biljaković, K.; Artemenko, S. N. Contribution of Charge-Density-Wave Phase Excitations to Thermal Conductivity Below the Peierls Transition. *Phys. Rev. B: Condens. Matter Mater. Phys.* **1993**, 48, 4329–4334.
- (31) Chen, J.; Hamann, D. M.; Choi, D. S.; Poudel, N.; Shen, L.; Shi, L.; Johnson, D. C.; Cronin, S. B. Enhanced Cross-plane Thermoelectric Transport of Rotationally-disordered SnSe₂ via Se Vapor Annealing. *Nano Lett.* **2018**, *18*, 6876–6881.
- (32) Tani, T.; Okajima, K.; Itoh, T.; Tanaka, S. Electronic transport properties in 1T-TaS₂. *Physica B+C* **1981**, *105*, 127–131.
- (33) Tani, T.; Tanaka, S. Thermoelectric Power Observation of Nearly-Commensurate Charge-Density Wave Phase in 1T-TaS₂. *J. Phys. Soc. Jpn.* **1984**, *53*, 1790–1796.
- (34) Bhatt, R.; Bhattacharya, S.; Basu, R.; Ahmad, S.; Chauhan, A. K.; Okram, G. S.; Bhatt, P.; Roy, M.; Navaneethan, M.; Hayakawa, Y.; Debnath, A. K.; Singh, A.; Aswal, D. K.; Gupta, S. K. Enhanced Thermoelectric Properties of Selenium-Deficient Layered TiSe_{2-x}: A Charge-Density-Wave Material. ACS Appl. Mater. Interfaces **2014**, 6, 18619–18625.
- (35) Huang, S. H.; Shu, G. J.; Pai, W. W.; Liu, H. L.; Chou, F. C. Tunable Se vacancy defects and the unconventional charge density wave in $1T-TiSe_{2-\delta}$. Phys. Rev. B: Condens. Matter Mater. Phys. **2017**, 95, 045310.
- (36) Naik, I.; Rastogi, A. K. Transport properties of 2H-NbSe2: Effect of Ga-intercalation. *Phys. B* **2010**, 405, 955–957.